

# Toward Better Target Representation for Source-Free and Black-Box Domain Adaptation

Qucheng Peng,<sup>1</sup> Zhengming Ding,<sup>2</sup> Lingjuan Lyu,<sup>3</sup> Lichao Sun,<sup>4</sup> Chen Chen<sup>1</sup>

<sup>1</sup> Center for Research in Computer Vision, University of Central Florida

<sup>2</sup> Tulane University, <sup>3</sup> Sony AI, <sup>4</sup> Lehigh University

qucheng.peng@knights.ucf.edu, chen.chen@crcv.ucf.edu

## Abstract

Domain adaptation aims at aligning the labeled source domain and the unlabeled target domain, and most existing approaches assume the source data is accessible. Unfortunately, this paradigm raises concerns in data privacy and security. Recent studies try to dispel these concerns by the Source-Free setting, which adapts the source-trained model towards target domain without exposing the source data. However, the Source-Free paradigm is still at risk of data leakage due to adversarial attacks to the source model. Hence, the Black-Box setting is proposed, where only the outputs of source model can be utilized. In this paper, we address both the Source-Free adaptation and the Black-Box adaptation, proposing a novel method named better target representation from Frequency Mixup and Mutual Learning (FMML). Specifically, we introduce a new data augmentation technique as Frequency MixUp, which highlights task-relevant objects in the interpolations, thus enhancing class-consistency and linear behavior for target models. Moreover, we introduce a network regularization method called Mutual Learning to the domain adaptation problem. It transfers knowledge inside the target model via self-knowledge distillation and thus alleviates overfitting on the source domain by learning multi-scale target representations. Extensive experiments show that our method achieves state-of-the-art performance on several benchmark datasets under both settings.

## 1. Introduction

Deep learning approaches have achieved remarkable success in various visual tasks (Noh, Hong, and Han 2015; Chen et al. 2017; Redmon et al. 2016; Ren et al. 2015) when there are large amount of labeled data and the training and test data lie in the same distribution. However, if the training and test data come from different domains, these methods cannot generalize well to the test domain due to the presence of *domain shift* (Ben-David et al. 2010). To alleviate this issue, domain adaptation (Wang and Deng 2018) is proposed to transfer knowledge from the labeled training data that form the *source* domain to the unlabeled test data that form the *target* domain. Most existing domain adaptation methods (Long et al. 2015; Tzeng et al. 2014; Sun and Saenko 2016; Ganin and Lempitsky 2015; Saito et al. 2018) need to access labeled data from source, but this paradigm cannot be satisfied under certain conditions (Kairouz et al. 2021). For example, personal medical reports from hospitals or personal

information records from social media must not be shared due to regulations that protect individual privacy. Therefore, a new setting –Source-Free domain adaptation (Liang, Hu, and Feng 2020)– emerges, where source data is completely unavailable when training on target. Even so, there are still potential risks if the source models are visible. Some works like dataset distillation (Wang et al. 2018) and DeepInversion (Yin et al. 2020) may recover data from the model through adversarial attacks. In such a case, Black-Box domain adaptation (Liang et al. 2021a) is introduced where the details of source models are completely unseen and only outputs of source models can be utilized for adaptation on target.

In a nutshell, only the target data and source models under different restrictions are available during the training on target for both Source-Free and Black-Box adaptation. To tackle this source-data absent problem, existing state-of-the-art methods mainly focus on developing solutions to align the two domains (i.e., source and target). For example, SHOT (Liang, Hu, and Feng 2020) uses information maximization and self-supervised pseudo-labeling to implicitly align representations of the two domains. A2Net (Xia, Zhao, and Ding 2021) leverages adversarial training to align two domains. SoFA (Yeh et al. 2021) adopts a mixture of Gaussian distributions as the reference distribution for target feature alignment. However, these methods do not explicitly align the distributions between the source and target domains for adaptation, and they may not be directly applicable to the more challenging Black-Box setting.

In this paper, we approach the problem from the perspective of *model regularization* to achieve domain adaptation and aim to answer the following question: *How to avoid model overfitting on the source pretraining?*

To tackle this challenge, we propose two modules (i.e. Frequency Mixup and Mutual Learning) to learn better target representations (i.e. better model generalization) in the adaptation stage *from the perspective of regularization* based on the available resources (target data and pre-trained model).

First, we build our intuition upon MixUp (Gidaris, Singh, and Komodakis 2018; Shorten and Khoshgoftaar 2019; Dorsch, Gupta, and Efros 2015; Zhang et al. 2018a), which regularizes ML model training from the data aspect, and develop a new and effective data augmentation method for domain adaptation as Frequency MixUp. Conventional MixUp directly blends one image’s pixels into another image (Wu,

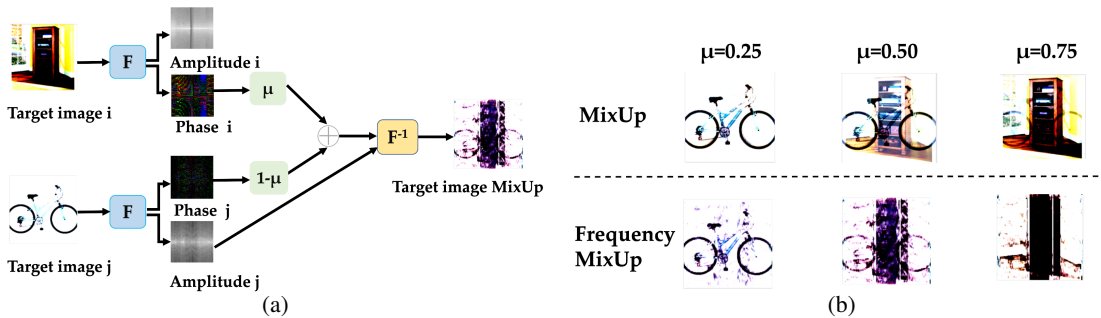


Figure 1: (a): Process of Frequency MixUp. (b): Comparisons between pixel-wise MixUp and our Frequency MixUp.

Inkpen, and El-Roby 2020; Liang et al. 2021a). During this process, the model learns not only sample information but also an interpolation function, which is called linear behavior (Zhang et al. 2018a). The linear combination encourages the smoothness of the model, and the smoothness can serve as prior knowledge to help the model learn better representations (Bengio, Courville, and Vincent 2013). But this kind of combination is too simple to highlight the task-relevant objects, especially when the image owns complex background and style information. For example, the top of Fig. 1b shows the MixUp between the “bookcase” image and the “bicycle” image. The “bookcase” image has relatively complex background (e.g. floor, window and even sunlight apart from the core object bookcase, see Fig. 1a) and style information. The goal of MixUp is to encourage model to learn linear behavior in-between objects hence learning better representations, so background elements will have a negative impact on MixUp as they distract the focus on core objects and the model tends to learn a linear behavior between the “bicycle” and the background instead. Frequency decomposition proves to be a useful tool to disentangle object information and background information from an image (Yang and Soatto 2020; Liu et al. 2021). Therefore, we propose Frequency MixUp (Fig. 1a) to capture the key objects and reduce environmental interference at the same time, as the bottom of Fig. 1b shows. By mixing their phase spectra, we can focus more on the two core objects “bicycle” and “bookcase” and weaken background information. The augmented image will attend further training to enhance the target model’s class-consistency.

Second, we introduce a self-knowledge distillation method called Mutual Learning to the domain adaptation problem. The goal is to regularize the model training on the target, so that better target representations can be learned. Some existing methods (Meng et al. 2018; Liang et al. 2021a) apply a teacher-student paradigm to transfer knowledge from source to target, and others like (Feng et al. 2021; Meng et al. 2018) distill knowledge from different sources. *These methods aim to explore knowledge from source models but this may lead to suboptimal performance due to domain shift. More importantly, the knowledge transfer inside the target network is overlooked.* We argue that it is essential to extract more target relevant knowledge for the model to adapt well on target distribution. Therefore, we introduce the idea of Mutual Learning (Zhang et al. 2018b; Yang et al. 2020) to the domain adaptation problem by transferring knowledge between different (network) parts of the target model. Rather than one-way transfer between source and target models, an ensemble of target network and its subnetworks learn collab-

oratively and teach each other, *which can be considered as regularization from the network structure aspect.* This process is achieved via self-knowledge distillation so that the target model is able to learn better target representations. We rescale the input resolutions, and slim the widths of network layers to get the subnetworks. By transferring knowledge between the original network and subnetworks mutually, the original network captures multi-scale representations from the target domain data and thus generalizes better on target.

**Connections between the Proposed Modules.** First, the proposed modules (Frequency MixUp and Mutual Learning) both aim to learn better target representations in the adaptation stage from the perspective of model regularization. Second, Frequency MixUp assists Mutual Learning. Specifically, the mutual learning strategy used in the paper leverages augmented inputs and multi-scale networks. In a way, this process can be regarded as a specific contrastive learning method, where stronger data augmentation is desired. The proposed Frequency MixUp, which adds disturbances to the raw data, benefits mutual learning in this regard. The proposed two modules work coherently to learn more generalizable and diverse target representations.

**Contribution.** Our contributions to Source-Free and Black-Box domain adaptation can be summarized in three aspects. *First*, we propose Frequency MixUp as a new data augmentation scheme that helps the model enhance class-consistency and linear behavior with more task-relevant object information and obtain better representations for the target domain. *Second*, we introduce Mutual Learning as a network regularization technique that assists the model to learn multi-scale representations and transfer knowledge between the model’s different parts mutually to avoid overfitting on source. *To the best of our knowledge, it is the first attempt to perform network regularization to the target model to achieve better domain adaptation*, which provides a new perspective. *Third*, extensive experimental results on three benchmark datasets show that our approach achieves state-of-the-art performance compared with the latest methods for both Source-Free and Black-Box domain adaptation.

## 2. Related Work

**Domain Adaptation.** Motivated by the theoretical work from (Ben-David et al. 2006, 2010), a flurry of domain adaptation methods have been proposed. Metric-based and GAN-based approaches are the two major routes in the single-source domain adaptation. Metric-based method tends to measure the discrepancy between the source and target do-

main explicitly. (Long et al. 2015) uses maximum mean discrepancy, while (Tzeng et al. 2014) applies deep domain confusion and (Sun and Saenko 2016) utilizes correlation relation. Recent work like (Wu et al. 2021) uses this paradigm to solve heterogeneous domain adaptation, and (Deng et al. 2021) jointly makes clustering and discrimination for alignment together with contrastive learning. The GAN-based method origins from (Goodfellow et al. 2014). It builds a min-max game for two players related to the source and target domains so as to minimize the discrepancy implicitly during the competition. (Ganin and Lempitsky 2015) adopts domain to confuse the two players, while (Saito et al. 2018) uses classifier discrepancy as the objective. (Xu et al. 2019) shows the importance of learning larger feature norms and (Tang, Chen, and Jia 2020) reveals that discriminative clustering on target will benefit the adaptation process.

**Source-Free Domain Adaptation.** The community pays more attention to the Source-Free setting owing to the concerns in data privacy, data portability and data transmission. Since (Li et al. 2020; Liang, Hu, and Feng 2020), Source-Free has become the mainstream paradigm for alleviating this concern, where sample-level source information is completely unseen during the training procedure on target. There are two technique routes under the source-free setting: self-supervision and virtual source transfer. For the self-supervised methods, (Liang, Hu, and Feng 2020) is the most representative, which introduces information maximization to assist. (Xia, Zhao, and Ding 2021) views this problem from a discriminative perspective and adds specific representation learning module to help the generalization. (Liang et al. 2021b) is an extended version of (Liang, Hu, and Feng 2020) and combines the merits from (Xia, Zhao, and Ding 2021). (Yang et al. 2021b) exploits the neighborhood structure to encourage class-wise consistency, while (Huang et al. 2021) constructs historical contrastive process to reweight target samples. (Chen et al. 2022) proposes the online pseudo label refinement and (Yang et al. 2021c) introduces attention modules to the network. Besides, (Yang et al. 2021a) replaces the backbones with vision transformer (Dosovitskiy et al. 2020). As for virtual source methods, most of them build GAN to generate virtual source data. (Kurmi et al. 2021) uses conditional GAN to generate new samples, while (Yeh et al. 2021) performs virtual cross-domain feature alignment. (Hou and Zheng 2021) provides interesting visualizations for unseen knowledge and (Li et al. 2020) applies collaborative GAN to achieve better generations. Part of our work belongs to this paradigm, where data and sample-based information from source is invisible during the target leverage, and here we choose the self-supervised route.

**Black-Box Domain Adaptation.** Black-Box domain adaptation is proposed by (Chang et al. 2019). It is a subset problem of Source-Free and also a very new topic. It is more strict than Source-Free because the models trained on source will be put into a black box and only the outputs of these models can be used when we turn to leverage on target. (Zhang et al. 2021) first states this setting completely and emphasizes on the purification of noisy labels. (Liang et al. 2021a) introduces knowledge distillation to the black-box problem, which largely improves the performance. Here we

also tackle this type of adaptation. All the details are kept the same as the Source-Free setting but the source model strictly follows the Black-Box rule.

### 3. Methodology

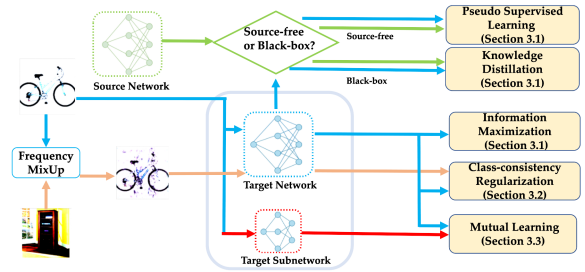


Figure 2: Overview of our proposed framework (Best viewed in color). The green part refers to source-related training, and the blue part refers to target-related training. Besides, we use orange and red colors to represent the process of Frequency MixUp and Mutual Learning, respectively.

#### 3.1 Preliminary

For a typical domain adaptation problem, we have a source domain dataset  $\mathcal{S} = \{(x_i^s, y_i^s)\}_{i=1}^{n_s}$  with  $n_s$  labeled samples. Besides, there exists a target domain dataset  $\mathcal{T} = \{x_i^t\}_{i=1}^{n_t}$  that includes  $n_t$  unlabeled samples. The source and target domains share the same label space  $\mathcal{D} = \{1, 2, \dots, K\}$  but lie in different distributions, where  $K$  is the number of classes.  $k$  here is a member of the label space. Our approach consists of two models, with source model as  $f_s$  and target model as  $f_t$ , and our goal is to seek the best model  $f_t$ . For both Source-Free and Black-Box paradigms, the optimization will start with the supervised learning on source as  $\mathcal{L}^s = -\mathbb{E}_{(x_i^s, y_i^s) \in \mathcal{S}} \sum_{k \in \mathcal{D}} l_i^s \log f_s(x_i^s)$  with label smoothing (Muller, Kornblith, and Hinton 2019):  $l_i^s = \alpha/K + (1 - \alpha)y_i^s$ . Besides, a widely-used information maximization objective is applied on target as (Liang, Hu, and Feng 2020; Liang et al. 2021a):

$$\begin{aligned} \mathcal{L}_{im} = & -\mathbb{E}_{x_i^t \in \mathcal{T}} \sum_{k \in \mathcal{D}} f_t(x_i^t) \log f_t(x_i^t) \\ & + \sum_{k \in \mathcal{D}} \mathbb{E}_{x_i^t \in \mathcal{T}} f_t(x_i^t) \log \mathbb{E}_{x_i^t \in \mathcal{T}} f_t(x_i^t), \end{aligned} \quad (1)$$

which relies on target data completely without cross-domain adaptation. Therefore, it is natural for us to consider knowledge transfer between the source model and the target model. The difference between Source-Free and Black-Box paradigms is the visibility of source model, so it is necessary to tackle them with distinctive strategies. Under Source-Free setting, source model's parameters are exposed, thus we are able to either transfer the model's weights or optimize directly to get high-quality pseudo label  $\hat{y}_i^t$ , then conduct pseudo-supervised learning:

$$\mathcal{L}_{ps} = -\mathbb{E}_{x_i^t \in \mathcal{T}} \sum_{k \in \mathcal{D}} \hat{y}_i^t \log f_t(x_i^t), \quad (2)$$

For Black-Box setting, source model's details are completely unseen except the model's output. In this case, knowledge

distillation (Hinton, Vinyals, and Dean 2015) is applied to transfer knowledge from source to target:

$$\mathcal{L}_{kd} = D_{\text{KL}}(P^T(x_i) || f_t(x_i^t)), \quad (3)$$

where  $D_{\text{KL}}(\cdot)$  denotes Kullback-Leibler (KL) Divergence and  $P^T(x_i)$  is the pseudo-label generated by adaptive label smoothing and exponential moving average. Readers are referred to (Liang et al. 2021a) for details.

### 3.2 Enhancing Class-Consistency via Frequency MixUp

Data augmentation via MixUp is a very popular technique in domain adaptation. Typically the goal is to enhance class-wise consistency and linear behavior by MixUp, thus helping the model learn better representations on target domain. Pixel-wise MixUp cannot highlight the task-relevant objects when the image has a complicated background, and it will lead to suboptimal performance since the core object may be ignored and the model learns a linear behavior between object and background instead. From the top of Fig. 1b, we can observe such drawback. We want to blend the ‘‘bookcase’’ object into the ‘‘bicycle’’ image. The ‘‘bookcase’’ sample here contains a relatively complex background with floor, window and even sunlight. These background elements have negative impacts on the MixUp effect. In this case, the core object ‘‘bookcase’’ is not focused and it is difficult for the model to learn a linear behavior between the ‘‘bicycle’’ and the ‘‘bookcase’’. Therefore, we propose Frequency MixUp to highlight the key objects and reduce environmental interference simultaneously. The bottom part of Fig. 1b illustrates the effect of Frequency MixUp, where the two core objects are highlighted.

We introduce the standard format of Fourier transform. Assume a target sample  $x_i^t \in \mathbb{R}^{C \times H \times W}$ , where  $C$ ,  $H$  and  $W$  correspond to channel numbers, height and width. We transfer it from RGB space to frequency space and then decompose its frequency as amplitude and phase:

$$\mathcal{F}_i^t = \sum_{h=0}^{H-1} \sum_{w=0}^{W-1} x_i^t \exp[-j2\pi(\frac{h}{H}u + \frac{w}{W}v)] = \mathcal{A}_i^t \exp(\mathcal{P}_i^t). \quad (4)$$

Here we ensure the one-to-one correspondence between channels of different spaces, while  $x_i^t$  is a function of the image pixel  $(h, w)$ , and  $\mathcal{F}_i^t$  is a function of the frequency spectrum unit  $(u, v)$ .  $\mathcal{A}_i^t$  is the amplitude spectrum and  $\mathcal{P}_i^t$  is the phase spectrum of the target sample  $x_i^t$ . According to (Yang and Soatto 2020; Liu et al. 2021), the amplitude spectrum reflects the low-level distributions like style and the high-level semantics like object shape are stored in the phase spectrum. Since our task here is domain adaptation for object recognition, we hope that our MixUp could learn a linear behavior more from core objects rather than the background. Hence, we interpolate between phase spectra as:

$$\mathcal{P}_{mix}^t = \mu \mathcal{P}_j^t + (1 - \mu) \mathcal{P}_i^t, \quad (5)$$

where  $\mathcal{P}_j^t$  is the phase spectrum from a randomly-selected target sample  $x_j^t$  as  $\mathcal{F}(x_j^t) = \mathcal{A}_j^t \exp(\mathcal{P}_j^t)$ , and  $\mu$  is sampled from a Beta distribution as  $Beta(0.3, 0.3)$ . After that, we

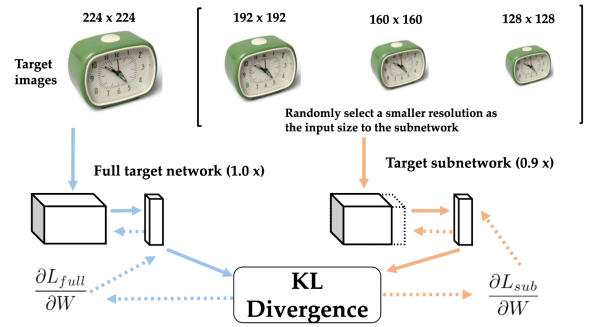


Figure 3: The training process of mutual learning (best viewed in color.) The left part with blue arrows reflects the training of original target network, and the right part with orange arrows shows the training of target subnetwork. During the optimization of  $L_{sub}$ , the model obtains knowledge of multi-scale target representations.

can get the Frequency MixUp augmented sample by inverse Fourier Transform:

$$\begin{aligned} x_{mix}^t &= \mathcal{F}^{-1}(\mathcal{A}_i^t, \mathcal{P}_{mix}^t) \\ &= \frac{1}{HW} \sum_{u=0}^{H-1} \sum_{v=0}^{W-1} \mathcal{A}_i^t \exp(\mathcal{P}_{mix}^t) \exp[-j2\pi(\frac{u}{H}h + \frac{v}{W}w)]. \end{aligned} \quad (6)$$

The Frequency MixUp procedure is shown in Fig. 1a. After obtaining the synthesized sample, we can enhance class-consistency by comparing the outputs of the original and synthesized samples. Here  $L_1$ -norm is utilized to compute the Frequency MixUp loss as:

$$\mathcal{L}_{mix} = \mathbb{E}_{x_i^t \in T} \|f_t(x_i^t) - f_t(x_{mix}^t)\|_{l_1}. \quad (7)$$

Frequency MixUp is different from conventional MixUp. Here Frequency MixUp serves as a small perturbation, because with appropriate disturbances, the target representations can be robust and more generalizable. And that is the reason why we set the Beta distribution’s parameter to be small enough as 0.3. In such a case, the disturbance is controllable and our augmented outputs can be consistent with the original outputs.

### 3.3 Encouraging Knowledge Transfer via Mutual Learning

During the procedure of knowledge transfer between source and target models, overfitting on source is an obvious side-effect. Hence, it is necessary to enforce target regularization to alleviate this issue. What’s more, previous works only consider the knowledge transfer from the source model to the target model. *The knowledge transfer inside the target model is overlooked.* To this end, we introduce the Mutual Learning strategy (Yang et al. 2020) to domain adaptation, which trains the target network and its subnetworks using multiple input (image) resolutions to learn multi-scale representations. Here we hope that this structure can assist the model to obtain more target information from diverse representations, thus overcoming overfitting on source.

We denote the target network’s weights as  $W$ . By slimming the network width with a ratio  $\alpha \in (0, 1]$ , subnetworks can be generated (Yang et al. 2020). A subnetwork with  $W_{0:\alpha}$  means selecting the first  $\alpha \times 100\%$  weights of each layer of

the full network. As we aim to avoid overfitting on source, it is meaningful to provide multi-scale representations from target as diverse receptive fields, by leveraging inputs with multiple resolutions. The resolution set  $\mathcal{R} = \{r_1 \times r_1, r_2 \times r_2, r_3 \times r_3\}$  consists of three resolutions satisfying  $0 < r_1, r_2, r_3 < 224$ .  $I_r$  requires input resolution as  $r \times r \in \mathcal{R}$ . Therefore, the network’s output with width  $\alpha$  and input size  $r \times r$  is denoted as  $f_t(x_i^t; W_{0:\alpha}; I_r)$ . Our goal is to mutually learn diverse multi-scale target representations via self-knowledge distillation between the target network and its subnetwork, thus assisting the network to generalize better on target. The Mutual Learning objective is defined as

$$\mathcal{L}_{ml} = \text{D}_{\text{KL}}(f_t(x_i^t; W_{0:\alpha}; I_r) || f_t(x_i^t; W_{0:1}; I_{224})), \quad (8)$$

where we randomly select  $r \times r$  from  $\mathcal{R}$  and then feed the resized samples into subnetwork. After getting these outputs from subnetwork with smaller width and input resolution, we compare them with the original network’s outputs using KL divergence. The procedures and details are in Fig. 3. Resolutions are set as 224, 192, 160, and 128, while subnetwork width is set as  $\alpha = 0.9 \times$ . Considering the efficiency and the complexity of parameter tuning, we just use one subnetwork here. When it comes to inference, we use the full network of target model with the original input scale.

Simply showing Eq. 8 is not persuasive enough to explain the effectiveness of learning multi-scale representations from subnetworks. Therefore, we illustrate it with a specific instance, which shows how mutual learning provides more target information so as to avoid source overfitting. Assume  $r \in \mathcal{R}$  and  $\alpha \in (0, 1]$ , then we denote the full target network and the target subnetwork as  $f_t(\cdot; W_{0:1}; I_{224})$  and  $f_t(\cdot; W_{0:\alpha}; I_r)$ . First, we show the gradients of full network:

$$\frac{\partial L_{full}}{\partial W} = \frac{\partial l_{W_{0:1}; I_{224}}}{\partial W_{0:1}} = \frac{\partial l_{W_{0:1}; I_{224}}}{\partial W_{0:\alpha}} \oplus \frac{\partial l_{W_{0:1}; I_{224}}}{\partial W_{\alpha:1}}, \quad (9)$$

where  $\oplus$  means vector concatenations. The reason why we can make such a decomposition is that  $W_{0:\alpha}$  and  $W_{0:1}$  share the part  $W_{0:\alpha}$ . After that, new content from subnetwork will be added to the optimization procedure to check whether it is able to improve the representation learning on target:

$$\begin{aligned} \frac{\partial L_{sub}}{\partial W} + \frac{\partial L_{full}}{\partial W} &= \frac{\partial l_{W_{0:\alpha}; I_r}}{\partial W_{0:\alpha}} + \frac{\partial l_{W_{0:1}; I_{224}}}{\partial W_{0:1}} \\ &= \frac{\partial l_{W_{0:\alpha}; I_r}}{\partial W_{0:\alpha}} + \frac{\partial l_{W_{0:1}; I_{224}}}{\partial W_{0:\alpha}} \oplus \frac{\partial l_{W_{0:1}; I_{224}}}{\partial W_{\alpha:1}} \\ &= \left( \frac{\partial l_{W_{0:\alpha}; I_r}}{\partial W_{0:\alpha}} + \frac{\partial l_{W_{0:1}; I_{224}}}{\partial W_{0:\alpha}} \right) \oplus \frac{\partial l_{W_{0:1}; I_{224}}}{\partial W_{\alpha:1}}. \end{aligned} \quad (10)$$

By comparing Eq. 9 and Eq. 10, we can clearly observe that difference comes from the first term inside the bracket of Eq. 10. This term provides multi-scale *target-based* knowledge from diverse receptive fields and gradients, thus can serve as a regularizer to alleviate overfitting on source, i.e. better generalization on target domain.

### 3.4 Overall Objectives

Our work considers two settings with different restrictions on source models, including Source-Free domain adaptation and

Black-Box domain adaptations. For Source-Free adaptation, the total loss is:

$$\mathcal{L}_{sf} = \mathcal{L}_{im} + \mathcal{L}_{ps} + \beta_1 \mathcal{L}_{mix} + \gamma_1 \mathcal{L}_{ml}. \quad (11)$$

For Black-Box adaptation, the final objective is:

$$\mathcal{L}_{bb} = \mathcal{L}_{im} + \mathcal{L}_{kd} + \beta_2 \mathcal{L}_{mix} + \gamma_2 \mathcal{L}_{ml}. \quad (12)$$

The first two items of each formula are inherited from (Liang et al. 2021b) and (Liang et al. 2021a).  $\beta_1, \gamma_1$  and  $\beta_2, \gamma_2$  are trade-off hyperparameters for corresponding loss functions.

## 4. Experiments

**Datasets.** For both Source-Free and Black-Box paradigms, we use three popular benchmark datasets for evaluation. **Office-31** (Saenko et al. 2010) has three domains as Amazon, Webcam, and DSLR with 31 classes and 4,652 images. **Office-Home** (Venkateswara et al. 2017) is a medium-size dataset, containing four domains as Art, Clipart, Product, and Real World. Each domain includes 65 classes and the total number of images is 15,500. **VisDA-C** (Peng et al. 2017) is the most challenging dataset among the three, though it only contains two domains. There are 152,000 synthesized images served as the source domain and 55,000 real images served as the target domain, each with 12 classes.

**Model Architecture.** For the neural network architecture of Source-Free paradigm, we adopt ResNet-50 (He et al. 2016) as the backbone for Office-31 and Office-Home, and ResNet-101 for VisDA-C. To facilitate fair comparisons, we follow the protocols from SHOT (Liang, Hu, and Feng 2020), replacing the last layer of ResNet with a pipeline as fully-connected layer, batch normalization layer, fully-connected layer and weight normalization layer. For the network architecture of Black-Box paradigm, same ResNets are applied for both source and target client as the backbones. What differs from Source-Free paradigm is that the model trained on source is almost the same as the original ResNet, with only the number of classes changed, while the model trained on target adopts the pipeline we mentioned above. This Black-Box setting follows the protocols from DINE (Liang et al. 2021a).

**Implementation.** For both the Source-Free and Black-Box paradigms, the same training strategy is used. We set the batch size to 64 and adopt SGD (Ruder 2016) as the optimizer, with a momentum of 0.9 and a weight decay of  $1e-3$ . For Office-31 and Office-Home, the learning rate is set as  $1e-3$  for the convolutional layers and  $1e-2$  for the rest. For VisDA-C, we choose  $1e-4$  for the convolutional layers and  $1e-3$  for the rest. The learning rate scheduler is the same as (Liang, Hu, and Feng 2020), i.e., a polynomial annealing strategy. Label smoothing (Muller, Kornblith, and Hinton 2019) is used on the leverage of source client, with 100 epochs for all the tasks. For the training procedure on target client, we train 30 epochs for all the tasks. In the evaluation stage, all results are obtained by averaging three random runs. For the hyper-parameters in Eqs. 11 and 12, we set  $\beta_1 = \beta_2 = 2$ ,  $\gamma_1 = 0.6$ , and  $\gamma_2 = 0.2$ . PyTorch (Paszke et al. 2019) is used for the implementation. For the proposed Mutual Learning (Sec. 3.3), the input resolutions are set as  $\{224, 192, 160, 128\}$ , while the subnetwork width is set as  $0.9 \times$ . When it

Table 1: **Source-Free** Domain Adaptation Accuracy (%) on (a) Office-31, (b) Office-Home, and (c) VisDA-C

(a) Office-31								Avg.						
	A→D	A→W	D→A	D→W	W→A	W→D								
Source-only	80.8	76.9	60.3	95.3	63.6	98.7		79.3						
SFDA	92.2	91.1	71.0	98.2	71.2	99.5		87.2						
SDDA	85.3	82.5	66.4	99.0	67.7	99.8		83.5						
SoFA	73.9	71.7	53.7	96.7	54.6	98.2		74.8						
SHOT	94.0	90.1	74.7	98.4	74.3	99.9		88.6						
CPGA	94.4	94.1	76.0	98.4	76.6	99.8		89.9						
VAKDT	89.9	91.8	73.9	98.7	72.0	99.9		87.7						
MA	92.7	93.7	75.3	98.5	77.8	99.8		89.6						
A2Net	94.5	94.0	76.7	99.2	76.1	<b>100</b>		90.1						
SHOT++	94.3	90.4	76.2	98.7	75.8	99.9		89.2						
NRC	<b>96.0</b>	90.8	75.3	99.0	75.0	<b>100</b>		89.4						
HCL	94.7	92.8	76.1	99.0	<b>78.3</b>	<b>100</b>		90.1						
<b>FMML</b>	<b>95.8±0.20</b>	<b>95.6±0.10</b>	<b>77.8±0.07</b>	<b>99.5±0.10</b>	77.7±0.07	<b>100±0.00</b>		<b>91.1±0.03</b>						
(b) Office-Home													Avg.	
	Ar→Cl	Ar→Pr	Ar→Rw	Cl→Ar	Cl→Pr	Cl→Rw	Pr→Ar	Pr→Cl	Pr→Rw	Rw→Ar	Rw→Cl	Rw→Pr		
Source-only	44.6	67.3	74.8	52.7	62.7	64.8	53.0	40.6	73.2	65.3	45.4	78.0		60.2
SFDA	48.4	73.4	76.9	64.3	69.8	71.7	62.7	45.3	76.6	69.8	50.5	79.0		65.7
SHOT	57.7	79.1	81.5	67.9	77.9	77.8	68.1	55.8	82.0	72.8	59.7	84.4		72.0
A2Net	58.4	79.0	82.4	67.5	79.3	78.9	68.0	56.2	82.9	<b>74.1</b>	60.5	85.0		72.8
NRC	57.7	80.3	82.0	68.1	79.8	78.6	65.3	56.4	<b>83.0</b>	71.0	58.6	85.6		72.2
SHOT++	57.9	79.7	82.5	68.5	79.6	79.3	68.5	57.0	<b>83.0</b>	73.7	60.7	84.9		73.0
<b>FMML</b>	<b>59.8±0.02</b>	<b>81.5±0.02</b>	<b>83.8±0.02</b>	<b>69.6±0.04</b>	<b>80.4±0.02</b>	<b>81.1±0.02</b>	<b>69.7±0.04</b>	<b>58.8±0.02</b>	82.9±0.02	73.2±0.04	<b>61.3±0.02</b>	<b>85.8±0.02</b>		<b>74.1±0.02</b>
(c) VisDA-C														Avg.
	plane	bicycl	bus	car	horse	knife	mcycl	person	plant	sktbrd	train	truck		
Source-only	60.9	21.6	50.9	67.6	65.8	6.3	82.2	23.2	57.3	30.6	84.6	8.0		46.6
SFDA	86.9	81.7	84.6	63.9	93.1	91.4	86.6	71.9	84.5	58.2	74.5	42.7		76.7
SHOT	95.8	88.2	87.2	73.7	95.2	96.4	87.9	84.5	92.5	89.3	85.7	49.1		85.5
CPGA	94.8	83.6	79.7	65.1	92.5	94.7	90.1	82.4	88.8	88.0	88.9	<b>60.1</b>		84.1
VAKDT	94.3	79.0	84.9	63.6	92.6	92.0	88.4	79.1	92.2	79.8	87.6	43.0		81.4
MA	95.7	78.0	69.0	74.2	94.6	93.0	88.0	87.2	92.2	88.8	85.1	54.3		83.3
A2Net	94.0	87.8	85.6	66.8	93.7	95.1	85.8	81.2	91.6	88.2	86.5	56.0		84.3
NRC	96.8	<b>91.3</b>	82.4	62.4	96.2	95.9	86.1	80.6	94.8	94.1	90.4	59.7		85.9
HCL	94.3	87.0	82.6	70.6	92.0	93.2	87.0	80.6	89.6	86.8	84.6	58.7		83.9
SHOT++	97.7	88.4	90.2	86.3	<b>97.9</b>	<b>98.6</b>	<b>92.9</b>	<b>84.1</b>	<b>97.1</b>	92.2	93.6	28.8		87.3
AdaContrast	97.0	84.7	84.0	77.3	96.8	93.8	91.9	<b>84.8</b>	94.3	<b>93.1</b>	94.1	49.7		86.8
<b>FMML</b>	<b>95.7±0.03</b>	<b>88.8±0.03</b>	<b>91.5±0.02</b>	<b>86.9±0.02</b>	<b>90.9±0.02</b>	<b>94.8±0.05</b>	<b>92.9±0.02</b>	<b>84.8±0.03</b>	<b>92.0±0.02</b>	<b>88.5±0.04</b>	<b>94.2±0.02</b>	<b>55.7±0.02</b>		<b>88.1±0.03</b>

comes to inference, we only use the full network model with the original input scale. Training is conducted on a NVIDIA GeForce RTX 3080 Ti GPU.

**Baselines.** Several state-of-the-art baselines are selected for comparisons. For the Source-Free paradigm, we compare our method with SFDA (Kim et al. 2020), SDDA (Kurmi et al. 2021), SoFA (Yeh et al. 2021), SHOT (Liang, Hu, and Feng 2020), CPGA (Qiu et al. 2021), VAKDT (Hou and Zheng 2021), MA (Li et al. 2020), A2Net (Xia, Zhao, and Ding 2021), SHOT++ (Liang et al. 2021b), AdaContrast (Chen et al. 2022), NRC (Yang et al. 2021b), and HCL (Huang et al. 2021). Two methods G-SFDA (Yang et al. 2021c) and TransDA (Yang et al. 2021a) are excluded since they introduce attention module to the backbones, which may lead to unfair comparisons. Under the Black-Box setting, we compare our method with NLL-OT (YM., C., and A. 2020), NLL-KL (Zhang et al. 2021), HD-SHOT (Liang, Hu, and Feng 2020), SD-SHOT (Liang, Hu, and Feng 2020), DINE (Liang et al. 2021a), and DINE-full (Liang et al. 2021a).

## 4.1 Results

**Source-Free Adaptation.** We compare our method (FMML) with existing Source-Free approaches and the results on three datasets are shown in Table 1. Based on the average accuracies on these datasets, our model achieves the state-of-the-art performances. Comparing with the second best approaches such as HCL on Office-31 and SHOT++ on Office-Home and VisDA-C, our method (FMML) gains improvements of 1.0%, 1.1%, and 0.8% correspondingly. When examining specific tasks, our approach outperforms all the competing baselines on 4 out of 6 tasks on Office-31, 10 out of 12 tasks on Office-Home, and 5 out of 12 tasks on VisDA-C.

**Black-Box Adaptation.** We also compare our method (FMML) with the existing Black-Box approaches and the results are reported in Table 2. For the average accuracies

on three datasets, our model again achieves the state-of-the-art performances. Comparing with the second best approach DINE-full on three datasets, our method yields improvements of 0.5%, 0.7%, and 0.4%, respectively. As for specific tasks, our approach outperforms all the listed baselines on 4 out of 6 tasks on Office-31, 11 out of 12 tasks on Office-Home, and 5 out of 12 tasks on VisDA-C.

## 4.2 Analysis

**Ablation Study.** We study the contributions of two proposed components in our approach and the results are shown in Table 3. Three representative tasks from different datasets are selected, as  $A \rightarrow D$ ,  $Ar \rightarrow Rw$ , and  $Syn \rightarrow Real$ .  $\mathcal{L}_{mix}$  refers to the loss from Frequency MixUp and  $\mathcal{L}_{ml}$  is the loss of Mutual Learning. Each time we remove one or two of these components to obtain the four variants. Table 3 reports the results under Source-Free setting. For Black-Box we put the results in the *supplementary*. From this table we can see that any removal of these two parts will lead to worse performance. Frequency MixUp plays a more significant role than Mutual Learning. Besides, from the task  $A \rightarrow D$  we observe that the cooperation of these two components lead to a better result (+1.5%) than the sum of improvements (+1.2%), *indicating that they are not independent modules and can work synergistically*.

As the proposed Frequency MixUp can be considered as a general data augmentation scheme, we further validate its superiority by comparing it with the existing state-of-the-art augmentation methods including MixUp (Zhang et al. 2018a), CutMix (Yun et al. 2019) and RandAugment (Shorten and Khoshgoftaar 2019). The comparison results of Source-Free are presented in Table 4 and those of Black-Box are in the *supplementary*. It is evident that Frequency MixUp consistently outperforms all the other three techniques.

**Parameter Study.** There are four hyper-parameters in our

Table 2: **Black-Box** Domain Adaptation Accuracy (%) on (a) Office-31, (b) Office-Home, and (c) VisDA-C

(a) Office-31		A→D	A→W	D→A	D→W	W→A	W→D	Avg.						
Source-only		79.9	76.6	56.4	92.8	60.9	98.5	77.5						
NLL-OT		88.8	85.5	64.6	95.1	66.7	98.7	83.2						
NLL-KL		89.4	86.8	65.1	94.8	67.1	98.7	83.6						
HD-SHOT		86.5	83.1	66.1	95.1	68.9	98.1	83.0						
SD-SHOT		89.2	83.7	67.9	95.3	71.1	97.1	84.1						
DINE		91.6	86.8	72.2	96.2	73.3	<b>98.6</b>	86.4						
DINE-full		91.7	87.5	72.9	<b>96.3</b>	73.7	98.5	86.7						
<b>FMML</b>	<b>93.0±0.20</b>	<b>88.2±0.10</b>	<b>73.5±0.07</b>	<b>95.8±0.10</b>	<b>74.4±0.07</b>	<b>98.5±0.20</b>	<b>87.2±0.05</b>							
(b) Office-Home		Ar→Cl	Ar→Pr	Ar→Rw	Cl→Ar	Cl→Pr	Cl→Rw	Pr→Ar	Pr→Cl	Pr→Rw	Rw→Ar	Rw→Cl	Rw→Pr	Avg.
Source-only		44.1	66.9	74.2	54.5	63.3	66.1	52.8	41.2	73.2	66.1	46.7	77.5	60.6
NLL-OT		49.1	71.7	77.3	60.2	68.7	73.1	57.0	46.5	76.8	67.1	52.3	79.5	64.9
NLL-KL		49.0	71.5	77.1	59.0	68.7	72.9	56.4	46.9	76.6	66.2	52.3	79.1	64.6
HD-SHOT		48.6	72.8	77.0	60.7	70.0	73.2	56.6	47.0	76.7	67.5	52.6	80.2	65.3
SD-SHOT		50.1	75.0	78.8	63.2	72.9	76.4	60.0	48.0	79.4	69.2	54.2	81.6	67.4
DINE		52.2	78.4	81.3	65.3	76.6	78.7	62.7	49.6	82.2	69.8	55.8	84.2	69.7
DINE-full		54.2	77.9	81.6	<b>65.9</b>	77.7	79.9	64.1	50.5	82.1	71.1	58.0	84.3	70.6
<b>FMML</b>	<b>55.0±0.02</b>	<b>78.5±0.02</b>	<b>82.8±0.02</b>	<b>65.4±0.04</b>	<b>78.7±0.02</b>	<b>80.1±0.02</b>	<b>64.7±0.04</b>	<b>51.2±0.02</b>	<b>83.0±0.02</b>	<b>72.4±0.04</b>	<b>58.6±0.02</b>	<b>84.6±0.02</b>	<b>71.3±0.02</b>	
(c) VisDA-C		plane	bicycl	bus	car	horse	knife	mcycl	person	plant	sktbrd	train	truck	Avg.
Source-only		64.3	24.6	47.9	75.3	69.6	8.5	79.0	31.6	64.4	31.0	81.4	9.2	48.9
NLL-OT		82.6	84.1	76.2	44.8	90.8	39.1	76.7	72.0	82.6	81.2	82.7	50.6	72.0
NLL-KL		82.7	83.4	76.7	44.9	90.9	38.5	78.4	71.6	82.4	80.3	82.9	50.4	71.9
HD-SHOT		75.8	85.8	78.0	43.1	92.0	41.0	79.9	78.1	84.2	86.4	81.0	<b>65.5</b>	74.2
SD-SHOT		79.1	85.8	77.2	43.4	91.6	41.0	<b>80.0</b>	<b>78.3</b>	<b>84.7</b>	<b>86.8</b>	81.1	65.1	74.5
DINE		81.4	86.7	77.9	<b>55.1</b>	92.2	34.6	<b>80.8</b>	<b>79.9</b>	87.3	87.9	84.3	58.7	75.6
DINE-full		<b>95.3</b>	85.9	80.1	53.4	93.0	37.7	80.7	79.2	86.3	<b>89.9</b>	85.7	60.4	77.3
<b>FMML</b>	<b>94.0±0.03</b>	<b>86.8±0.03</b>	<b>79.0±0.02</b>	<b>55.0±0.02</b>	<b>93.5±0.02</b>	<b>42.3±0.05</b>	<b>80.2±0.02</b>	<b>78.6±0.03</b>	<b>87.7±0.02</b>	<b>89.5±0.04</b>	<b>86.8±0.02</b>	<b>59.5±0.02</b>	<b>77.7±0.03</b>	

Table 3: Ablation Study under Source-Free Setting

Method	A→D	Ar→Rw	Syn→Real
w/o $\mathcal{L}_{mix}$ & $\mathcal{L}_{ml}$ (baseline)	94.3	82.5	87.3
w/ $\mathcal{L}_{mix}$	95.2 (↑ 0.9)	83.5 (↑ 1.0)	87.9 (↑ 0.6)
w/ $\mathcal{L}_{ml}$	94.6 (↑ 0.3)	82.8 (↑ 0.3)	87.5 (↑ 0.2)
<b>FMML (<math>\mathcal{L}_{mix}</math> + <math>\mathcal{L}_{ml}</math>)</b>	<b>95.8 (↑ 1.5)</b>	<b>83.8 (↑ 1.3)</b>	<b>88.1 (↑ 0.8)</b>

Table 4: Comparison of Different Augmentation Methods for Source-Free Domain Adaptation

Method	A→D	Ar→Cl	Syn→Real
SHOT	94.0	57.7	85.5
SHOT w/ MixUp	93.9 (-0.1)	57.7 (+0.0)	85.5 (+0.0)
SHOT w/ CutMix	93.8 (-0.2)	56.5 (-1.2)	84.5 (-1.0)
SHOT w/ RandAugment	94.1 (+0.1)	58.0 (+0.3)	85.7 (+0.2)
SHOT w/ <b>Frequency MixUp</b>	<b>94.8 (+0.8)</b>	<b>58.8 (+1.1)</b>	<b>86.2 (+0.7)</b>
SHOT++	94.3	57.9	87.3
SHOT++ w/ MixUp	94.5 (+0.2)	58.4 (+0.5)	86.8 (-0.5)
SHOT++ w/ CutMix	93.6 (-0.7)	56.9 (-1.0)	86.4 (-0.9)
SHOT++ w/ RandAugment	94.5 (+0.2)	58.0 (+0.1)	87.3 (+0.0)
SHOT++ w/ <b>Frequency MixUp</b>	<b>95.2 (+0.9)</b>	<b>59.4 (+1.5)</b>	<b>87.9 (+0.6)</b>
NRC	92.0	57.7	72.9
NRC w/ MixUp	92.2 (+0.2)	58.0 (+0.3)	72.7 (-0.2)
NRC w/ CutMix	91.8 (-0.2)	57.4 (-0.3)	72.5 (-0.4)
NRC w/ RandAugment	92.0 (+0.0)	57.7 (+0.0)	73.0 (+0.1)
NRC w/ <b>Frequency MixUp</b>	<b>92.5 (+0.5)</b>	<b>58.4 (+0.7)</b>	<b>73.3 (+0.4)</b>

two overall objectives (Eqs. 11 and 12) as  $\beta_1$ ,  $\gamma_1$ ,  $\beta_2$  and  $\gamma_2$  that weight the importance of  $\mathcal{L}_{mix}$  and  $\mathcal{L}_{ml}$ . We select the task Art→Clipart from Office-Home and conduct parameter analysis in Fig. 4. For  $\beta_1$  and  $\beta_2$ , we choose relatively large values with an interval of 0.2, while for  $\gamma_1$  and  $\gamma_2$  the values are smaller with an interval of 0.04. From this figure we can observe that the best values for  $\beta_1$  and  $\beta_2$  are near 2.0 and 2.2. For  $\gamma_1$ , 0.48 to 0.60 is a suitable range, and 0.20 to 0.28 for  $\gamma_2$ . What’s more, we can see that the model’s performance remains stable (i.e., small fluctuations within 0.3) and competitive in the range of values we tested.

We also provide a detailed analysis on the sub-network width in Mutual Learning based on both Source-Free and Black-Box settings with task Art→Clipart, as shown in Table 5. We see that the best choice for Source-Free is between 0.90 and 0.94, while it is between 0.86 and 0.92 for Black-Box. Our choice of using 0.9 is reasonable. Besides, we observe that subnetwork width = 1.0 cannot achieve the best results. This is because if the subnetwork also has the width=1.0 (i.e. the same network as the full network), the structure regularization aspect of the Mutual Learning is completely lost. The multi-scale representation learning not only comes from the input (as shown in Fig. 3), but also comes from the

Table 5: FMML Analysis with Different Width Ratios of Sub-network

Width Ratios	0.80	0.82	0.84	0.86	0.88	0.90	0.92	0.94	0.96	0.98	1.00
Source-Free	59.45	59.50	59.50	59.63	59.73	59.77	59.82	59.68	59.56	59.47	59.45
Black-Box	54.87	54.89	54.93	54.96	55.02	55.01	54.94	54.91	54.89	54.87	54.85

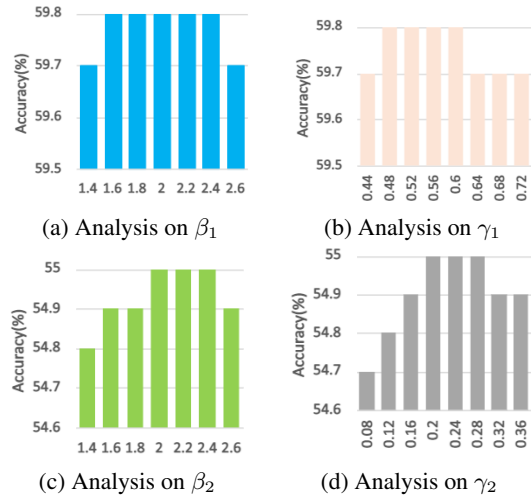


Figure 4: Parameter Analysis on task Art→Clipart from Office-Home (best viewed in color). **a**: Analysis on  $\beta_1$ . **b**: Analysis on  $\gamma_1$ . **c**: Analysis on  $\beta_2$ . **d**: Analysis on  $\gamma_2$ .

network structure by using the subnetwork (as we inspected the model gradients, i.e., Eqs. 9 and 10).

## 5. Conclusion

In this paper, we propose a method named Frequency Mixup and Mutual Learning (FMML) for Source-Free and Black-Box domain adaptation. We propose a new data augmentation technique called Frequency MixUp to encourage class-consistency and linear behavior for better target representations. We also introduce Mutual Learning structure as a network regularization technique to distill knowledge between the target network and its subnetwork, thus learning multi-scale target representations. Comprehensive results on three datasets testify FMML’s efficacy, together with analysis. As we mainly focus on target representations here, further work can be done by exploring more knowledge from source to gain improvements.

## References

- Ben-David, S.; Blitzer, J.; Crammer, K.; Kulesza, A.; Pereira, F.; and Vaughan, J. W. 2010. A theory of learning from different domains. *Machine Learning*, 151–175.
- Ben-David, S.; Blitzer, J.; Crammer, K.; and Pereira, F. 2006. Analysis of representations for domain adaptation. *Advances in Neural Information Processing Systems*.
- Bengio, Y.; Courville, A.; and Vincent, P. 2013. Representation learning: A review and new perspectives. *IEEE Transactions on Pattern Analysis and Machine Intelligence*, 35(8): 1798–1828.
- Chang, H.; Shejwalkar, V.; Shokri, R.; and Houmansadr, A. 2019. Cronus: Robust and heterogeneous collaborative learning with black-box knowledge transfer. *arXiv preprint arXiv:1912.11279*.
- Chen, D.; Wang, D.; Darrell, T.; and Ebrahimi, S. 2022. Contrastive Test-Time Adaptation. *arXiv preprint arXiv:2204.10377*.
- Chen, L.-C.; Papandreou, G.; Kokkinos, I.; Murphy, K.; and Yuille, A. L. 2017. Deeplab: Semantic image segmentation with deep convolutional nets, atrous convolution, and fully connected crfs. *IEEE Transactions on Pattern Analysis and Machine Intelligence*, 40(4): 834–848.
- Deng, W.; Liao, Q.; Zhao, L.; Guo, D.; Kuang, G.; Hu, D.; and Liu, L. 2021. Joint Clustering and Discriminative Feature Alignment for Unsupervised Domain Adaptation. *IEEE Transactions on Image Processing*, 7842–7855.
- Doersch, C.; Gupta, A.; and Efros, A. A. 2015. Unsupervised visual representation learning by context prediction. In *Proceedings of the IEEE International Conference on Computer Vision*, 1422–1430.
- Dosovitskiy, A.; Beyer, L.; Kolesnikov, A.; Weissenborn, D.; Zhai, X.; Unterthiner, T.; Dehghani, M.; Minderer, M.; Heigold, G.; Gelly, S.; et al. 2020. An image is worth 16x16 words: Transformers for image recognition at scale. *arXiv preprint arXiv:2010.11929*.
- Feng, H.-Z.; You, Z.; Chen, M.; Zhang, T.; Zhu, M.; Wu, F.; Wu, C.; and Chen, W. 2021. KD3A: Unsupervised multi-source decentralized domain adaptation via knowledge distillation. In *International Conference on Machine Learning*, 3274–3283. PMLR.
- Ganin, Y.; and Lempitsky, V. 2015. Unsupervised domain adaptation by backpropagation. In *International Conference on Machine Learning*, 1180–1189.
- Gidaris, S.; Singh, P.; and Komodakis, N. 2018. Unsupervised Representation Learning by Predicting Image Rotations. In *International Conference on Learning Representations*.
- Goodfellow, I.; Pouget-Abadie, J.; Mirza, M.; Xu, B.; Warde-Farley, D.; Ozair, S.; Courville, A.; and Bengio, Y. 2014. Generative adversarial nets. *Advances in Neural Information Processing Systems*, 27.
- He, K.; Zhang, X.; Ren, S.; and Sun, J. 2016. Deep residual learning for image recognition. In *Proceedings of the IEEE Conference on Computer Vision and Pattern Recognition*, 770–778.
- Hinton, G.; Vinyals, O.; and Dean, J. 2015. Distilling the Knowledge in a Neural Network. *STAT*.
- Hou, Y.; and Zheng, L. 2021. Visualizing adapted knowledge in domain transfer. In *Proceedings of the IEEE/CVF Conference on Computer Vision and Pattern Recognition*, 13824–13833.
- Huang, J.; Guan, D.; Xiao, A.; and Lu, S. 2021. Model adaptation: Historical contrastive learning for unsupervised domain adaptation without source data. *Advances in Neural Information Processing Systems*, 34.
- Kairouz, P.; McMahan, H. B.; Avent, B.; Bellet, A.; Bennis, M.; Bhagoji, A. N.; Bonawitz, K.; Charles, Z.; Cormode, G.; Cummings, R.; et al. 2021. Advances and open problems in federated learning. *Foundations and Trends® in Machine Learning*, 14(1–2): 1–210.
- Kim, Y.; Cho, D.; Han, K.; Panda, P.; and Hong, S. 2020. Domain adaptation without source data. *arXiv preprint arXiv:2007.01524*.
- Kurmi, V. K.; Subramanian, V. K.; Namboodiri, V. P.; and . 2021. Domain impression: A source data free domain adaptation method. In *Proceedings of the IEEE/CVF Winter Conference on Applications of Computer Vision*, 615–625.
- Li, R.; Jiao, Q.; Cao, W.; Wong, H.-S.; and Wu, S. 2020. Model Adaptation: Unsupervised Domain Adaptation Without Source Data. In *2020 IEEE/CVF Conference on Computer Vision and Pattern Recognition (CVPR)*, 9638–9647.
- Liang, J.; Hu, D.; and Feng, J. 2020. Do we really need to access the source data? source hypothesis transfer for unsupervised domain adaptation. In *International Conference on Machine Learning*, 6028–6039. PMLR.
- Liang, J.; Hu, D.; He, R.; and Feng, J. 2021a. Distill and fine-tune: Effective adaptation from a black-box source model. *arXiv preprint arXiv:2104.01539*.
- Liang, J.; Hu, D.; Wang, Y.; He, R.; and Feng, J. 2021b. Source data-absent unsupervised domain adaptation through hypothesis transfer and labeling transfer. *IEEE Transactions on Pattern Analysis and Machine Intelligence*.
- Liu, Q.; Chen, C.; Qin, J.; Dou, Q.; and Heng, P.-A. 2021. Feddg: Federated domain generalization on medical image segmentation via episodic learning in continuous frequency space. In *Proceedings of the IEEE/CVF Conference on Computer Vision and Pattern Recognition*, 1013–1023.
- Long, M.; Cao, Y.; Wang, J.; and Jordan, M. 2015. Learning transferable features with deep adaptation networks. In *International Conference on Machine Learning*, 97–105.
- Meng, Z.; Li, J.; Gong, Y.; and Juang, B.-H. 2018. Adversarial teacher-student learning for unsupervised domain adaptation. In *2018 IEEE International Conference on Acoustics, Speech and Signal Processing (ICASSP)*, 5949–5953. IEEE.
- Muller, R.; Kornblith, S.; and Hinton, G. E. 2019. When does label smoothing help? *Advances in Neural Information Processing Systems*.
- Noh, H.; Hong, S.; and Han, B. 2015. Learning deconvolution network for semantic segmentation. In *Proceedings of the IEEE International Conference on Computer Vision*, 1520–1528.
- Paszke, A.; Gross, S.; Massa, F.; Lerer, A.; Bradbury, J.; Chanan, G.; Killeen, T.; Lin, Z.; Gimelshein, N.; Antiga, L.; et al. 2019. Pytorch: An imperative style, high-performance deep learning library. *Advances in Neural Information Processing Systems*.
- Peng, X.; Usman, B.; Kaushik, N.; Hoffman, J.; Wang, D.; and Saenko, K. 2017. Visda: The visual domain adaptation challenge. *arXiv preprint arXiv:1710.06924*.
- Qiu, Z.; Zhang, Y.; Lin, H.; Niu, S.; Liu, Y.; Du, Q.; and Tan, M. 2021. Source-free Domain Adaptation via Avatar Prototype Generation and Adaptation. In Zhou, Z.-H., ed., *Proceedings of the International Joint Conference on Artificial Intelligence*, 2921–2927.
- Redmon, J.; Divvala, S.; Girshick, R.; and Farhadi, A. 2016. You only look once: Unified, real-time object detection. In *Proceedings of the IEEE Conference on Computer Vision and Pattern Recognition*, 779–788.
- Ren, S.; He, K.; Girshick, R.; and Sun, J. 2015. Faster r-cnn: Towards real-time object detection with region proposal networks. *Advances in Neural Information Processing Systems*, 28.
- Ruder, S. 2016. An overview of gradient descent optimization algorithms. *arXiv preprint arXiv:1609.04747*.



- Saenko, K.; Kulis, B.; Fritz, M.; and Darrell, T. 2010. Adapting visual category models to new domains. In *European Conference on Computer Vision*, 213–226.
- Saito, K.; Watanabe, K.; Ushiku, Y.; and Harada, T. 2018. Maximum classifier discrepancy for unsupervised domain adaptation. In *Proceedings of the IEEE Conference on Computer Vision and Pattern Recognition*, 3723–3732.
- Shorten, C.; and Khoshgoftaar, T. M. 2019. A survey on image data augmentation for deep learning. *Journal of Big Data*, 6(1): 1–48.
- Sun, B.; and Saenko, K. 2016. Deep coral: Correlation alignment for deep domain adaptation. In *European Conference on Computer Vision*, 443–450.
- Tang, H.; Chen, K.; and Jia, K. 2020. Unsupervised domain adaptation via structurally regularized deep clustering. In *Proceedings of the IEEE/CVF Conference on Computer Vision and Pattern Recognition*, 8725–8735.
- Tzeng, E.; Hoffman, J.; Zhang, N.; Saenko, K.; and Darrell, T. 2014. Deep domain confusion: Maximizing for domain invariance. *arXiv preprint arXiv:1412.3474*.
- Venkateswara, H.; Eusebio, J.; Chakraborty, S.; and Panchanathan, S. 2017. Deep hashing network for unsupervised domain adaptation. In *Proceedings of the IEEE Conference on Computer Vision and Pattern Recognition*, 5018–5027.
- Wang, M.; and Deng, W. 2018. Deep visual domain adaptation: A survey. *Neurocomputing*, 312: 135–153.
- Wang, T.; Zhu, J.-Y.; Torralba, A.; and Efros, A. A. 2018. Dataset distillation. *arXiv preprint arXiv:1811.10959*.
- Wu, H.; Zhu, H.; Yan, Y.; Wu, J.; Zhang, Y.; and Ng, M. K. 2021. Heterogeneous Domain Adaptation by Information Capturing and Distribution Matching. *IEEE Transactions on Image Processing*, 6364–6376.
- Wu, Y.; Inkpen, D.; and El-Roby, A. 2020. Dual mixup regularized learning for adversarial domain adaptation. In *European Conference on Computer Vision*, 540–555. Springer.
- Xia, H.; Zhao, H.; and Ding, Z. 2021. Adaptive Adversarial Network for Source-Free Domain Adaptation. In *Proceedings of the IEEE/CVF International Conference on Computer Vision*, 9010–9019.
- Xu, R.; Li, G.; Yang, J.; and Lin, L. 2019. Larger norm more transferable: An adaptive feature norm approach for unsupervised domain adaptation. In *Proceedings of the IEEE/CVF International Conference on Computer Vision*, 1426–1435.
- Yang, G.; Tang, H.; Zhong, Z.; Ding, M.; Shao, L.; Sebe, N.; and Ricci, E. 2021a. Transformer-based source-free domain adaptation. *arXiv preprint arXiv:2105.14138*.
- Yang, S.; van de Weijer, J.; Herranz, L.; Jui, S.; et al. 2021b. Exploiting the Intrinsic Neighborhood Structure for Source-free Domain Adaptation. *Advances in Neural Information Processing Systems*, 34.
- Yang, S.; Wang, Y.; van de Weijer, J.; Herranz, L.; and Jui, S. 2021c. Generalized Source-Free Domain Adaptation. In *Proceedings of the IEEE/CVF International Conference on Computer Vision (ICCV)*, 8978–8987.
- Yang, T.; Zhu, S.; Chen, C.; Yan, S.; Zhang, M.; and Willis, A. 2020. Mutualnet: Adaptive convnet via mutual learning from network width and resolution. In *European Conference on Computer Vision*, 299–315. Springer.
- Yang, Y.; and Soatto, S. 2020. Fda: Fourier domain adaptation for semantic segmentation. In *Proceedings of the IEEE/CVF Conference on Computer Vision and Pattern Recognition*, 4085–4095.
- Yeh, H.-W.; Yang, B.; Yuen, P. C.; and Harada, T. 2021. SoFA: Source-Data-Free Feature Alignment for Unsupervised Domain Adaptation. In *Proceedings of the IEEE/CVF Winter Conference on Applications of Computer Vision*, 474–483.
- Yin, H.; Molchanov, P.; Alvarez, J. M.; Li, Z.; Mallya, A.; Hoiem, D.; Jha, N. K.; and Kautz, J. 2020. Dreaming to distill: Data-free knowledge transfer via deepinversion. In *Proceedings of the IEEE/CVF Conference on Computer Vision and Pattern Recognition*, 8715–8724.
- YM., A.; C., R.; and A., V. 2020. Self-labelling via simultaneous clustering and representation learning. In *International Conference on Learning Representations*.
- Yun, S.; Han, D.; Oh, S. J.; Chun, S.; Choe, J.; and Yoo, Y. 2019. Cutmix: Regularization strategy to train strong classifiers with localizable features. In *Proceedings of the IEEE/CVF international conference on computer vision*, 6023–6032.
- Zhang, H.; Cisse, M.; Dauphin, Y. N.; and Lopez-Paz, D. 2018a. mixup: Beyond Empirical Risk Minimization. In *International Conference on Learning Representations*.
- Zhang, H.; Zhang, Y.; Jia, K.; and Zhang, L. 2021. Unsupervised domain adaptation of black-box source models. *arXiv preprint arXiv:2101.02839*.
- Zhang, Y.; Xiang, T.; Hospedales, T. M.; and Lu, H. 2018b. Deep mutual learning. In *Proceedings of the IEEE Conference on Computer Vision and Pattern Recognition*, 4320–4328.

# Toward Better Target Representation for Source-Free and Black-Box Domain Adaptation – Supplementary Material

Written by AAI Press Staff<sup>1</sup>\*

AAAI Style Contributions by Pater Patel Schneider, Sunil Issar,

J. Scott Penberthy, George Ferguson, Hans Guesgen, Francisco Cruz<sup>†</sup>, Marc Pujol-Gonzalez<sup>†</sup>

<sup>1</sup>Association for the Advancement of Artificial Intelligence  
1900 Embarcadero Road, Suite 101  
Palo Alto, California 94303-5310 USA  
publications23@aaai.org

## 1. Feature Visualization

Fig. 1 represents the t-SNE (?) visualization of feature representation on Amazon→DSLRL task from Office-31. Here three situations are selected for comparisons including pretrained ResNet-50, source-trained model, well-adapted Source-Free and Black-Box model. The red dots represent features of Amazon, while the blue dots represent features of DSLR. From the target part, we illustrate the effectiveness of our method, since it forms clear clusters in subfigure c and d, showing the improvement of target representations and the effectiveness of the adaptation process under both settings.

## 2. More Ablation Study Results

**Analysis of the proposed two modules.** In the main paper we present the ablation results of the proposed two components (Frequency MixUp and Mutual Learning) under the Source-Free setting. Here we also show the results for the Black-Box setting in Table 1. Since both situations are similar, we are not going to reiterate our conclusions.

Moreover, we did a complete set of experiments of all the tasks on three datasets to validate the effectiveness of the proposed two modules. The results are reported in Tables 2-7.

**Comparisons of Frequency MixUp with other data augmentation methods for Black-Box adaptation.** In the main paper, we show the comparisons of multiple data augmentation methods based on Source-Free setting. And here are the results for Black-Box as Table 8. From it we observe that Frequency MixUp outperforms all the other three augmentation methods, indicating its effectiveness.

Table 1: Ablation under Black-Box setting

Method	A → D	Ar → Rw	Syn → Real
w/o $\mathcal{L}_{mix}$ & $\mathcal{L}_{ml}$ (baseline)	91.7	81.6	77.3
w/ $\mathcal{L}_{mix}$	92.8 (↑ 1.1)	82.4 (↑ 0.8)	77.6 (↑ 0.3)
w/ $\mathcal{L}_{ml}$	92.0 (↑ 0.3)	81.9 (↑ 0.3)	77.3 (↑ 0.0)
FMML ( $\mathcal{L}_{mix} + \mathcal{L}_{ml}$ )	93.0 (↑ 1.3)	82.8 (↑ 1.2)	77.7 (↑ 0.4)

\*With help from the AAI Publications Committee.

<sup>†</sup>These authors contributed equally.

Table 2: Source-Free Domain Adaptation Accuracy (%) on Office-31 Dataset

Method	A → D	A → W	D → A	D → W	W → A	W → D	Avg.
Source-only	80.8	76.9	60.3	95.3	63.6	98.7	79.3
SFDA	92.2	91.1	71.0	98.2	71.2	99.5	87.2
SDDA	85.3	82.5	66.4	99.0	67.7	99.8	83.5
SDFB	73.9	71.7	53.7	96.7	54.6	98.2	74.8
SHOT	94.0	90.1	74.7	98.4	74.3	99.9	88.6
CPGA	94.4	94.1	76.0	98.4	76.6	99.8	89.9
VAKDT	89.9	91.8	73.9	98.7	72.0	99.9	87.7
MA	92.7	93.7	75.3	98.5	77.8	99.8	89.6
ANet	94.5	94.0	76.7	99.2	76.1	<b>100</b>	90.1
SHOT++	94.3	90.4	76.2	98.7	75.8	99.9	89.2
NRC	<b>96.0</b>	90.8	75.3	99.0	75.0	<b>100</b>	89.4
HCL	94.7	92.8	76.1	99.0	<b>78.3</b>	<b>100</b>	90.1
FMML w/o $\mathcal{L}_{mix}$	94.6±0.20	91.5±0.10	76.7±0.07	99.1±0.10	76.8±0.07	<b>100±0.00</b>	89.8±0.05
FMML w/o $\mathcal{L}_{ml}$	95.2±0.20	95.0±0.10	77.4±0.07	99.0±0.10	77.3±0.07	<b>100±0.00</b>	90.7±0.03
FMML	95.8±0.20	<b>95.6±0.10</b>	<b>77.8±0.07</b>	<b>99.5±0.10</b>	77.7±0.07	<b>100±0.00</b>	<b>91.1±0.03</b>

Table 3: Source-Free Domain Adaptation Accuracy (%) on Office-Home Dataset

Method	Ar → Cl	Ar → Pr	Ar → Rw	Cl → Ar	Cl → Pr	Cl → Rw	Pr → Ar	Pr → Cl	Pr → Rw	Rw → Ar	Rw → Cl	Rw → Pr	Avg.
Source-only	47.6	57.1	48.8	52.1	58.8	54.8	51.0	49.6	52.5	55.4	59.1	59.1	52.7
SFDA	48.4	73.4	76.9	64.3	69.8	71.7	62.7	45.3	76.6	69.8	50.5	79.0	65.7
SHOT	47.7	79.1	81.5	61.9	77.9	77.8	68.1	55.8	82.0	72.8	59.7	84.4	72.9
ANet	34.4	79.0	82.4	67.5	79.3	78.9	68.0	56.2	82.9	<b>74.1</b>	66.5	85.0	72.8
MA	37.7	80.3	82.0	68.1	79.8	78.6	65.3	56.4	<b>83.8</b>	71.0	55.5	85.6	72.2
SHOT++	37.9	79.7	82.5	68.5	79.6	79.3	68.5	57.0	<b>83.8</b>	71.7	60.7	84.9	73.0
FMML w/o $\mathcal{L}_{mix}$	89.8±0.02	79.8±0.02	82.8±0.02	68.8±0.02	79.9±0.02	79.8±0.02	69.0±0.01	59.8±0.02	<b>83.8±0.02</b>	71.4±0.01	61.0±0.01	85.2±0.02	73.9±0.02
FMML w/o $\mathcal{L}_{ml}$	91.8±0.02	81.4±0.02	83.4±0.02	69.3±0.01	80.2±0.02	80.5±0.02	69.2±0.01	58.4±0.02	82.9±0.02	73.1±0.01	61.1±0.02	85.5±0.02	75.7±0.02
FMML	93.8±0.02	<b>81.5±0.02</b>	<b>83.8±0.02</b>	<b>69.6±0.01</b>	<b>80.4±0.02</b>	<b>81.1±0.02</b>	<b>69.7±0.01</b>	<b>58.8±0.02</b>	82.9±0.02	73.2±0.01	<b>61.3±0.02</b>	<b>85.8±0.02</b>	<b>74.1±0.02</b>

## 4. Results of Partial-Set and Open-Set Domain Adaptation

In this section, we provide results for Partial-Set and Open-Set settings in Table 9-12. Here we use Office-Home dataset to do partial-set and open-set domain adaptation as previous work does and follow the protocols from SHOT (?). For partial-set, there are 65 classes in source and 25 classes in target, while for open-set, there are 25 classes in source and 65 classes in target including unknown samples. FMML outperforms SHOT++ by 0.9% for both Partial-Set and Open-Set, and it surpasses DINE-fill by 2.9% and 2.0% for Partial-Set and Open-Set separately. The results illustrate the effective-

Table 4: Source-Free Domain Adaptation Accuracy (%) on VisDA-C Dataset

Method	plane	bycel	bus	car	horse	knife	mycel	person	plant	skibed	train	truck	Mean
Source-only	60.9	31.6	30.9	69.6	65.8	6.3	82.2	23.2	37.8	30.6	81.6	8.0	46.6
SDFA	86.9	87.6	79.7	62.9	92.5	91.1	86.6	71.9	84.9	88.8	85.9	84.7	81.1
SHOT	95.8	88.2	87.2	73.7	95.2	96.4	87.9	84.5	92.5	89.3	85.7	49.1	85.5
CPGA	94.8	87.6	79.7	62.9	92.5	94.7	90.3	82.4	98.8	88.0	85.9	60.8	84.1
VAKDT	94.3	79.0	84.9	63.6	92.6	92.0	88.4	79.1	92.2	79.8	87.6	43.0	81.4
MA	95.7	78.9	80.0	74.2	94.6	93.0	88.0	87.2	92.2	88.8	85.1	54.3	83.3
ANet	94.0	87.8	85.6	66.8	93.7	95.1	85.8	81.2	91.6	88.2	86.5	56.0	84.3
NRC	96.8	<b>91.3</b>	82.4	62.4	96.2	95.9	86.1	80.6	94.8	94.1	90.4	59.7	85.9
HCL	94.3	87.0	82.6	70.6	92.0	93.2	87.0	80.6	89.6	86.8	84.6	58.7	83.9
SHOT++	97.7	88.4	90.2	86.3	<b>97.9</b>	<b>98.6</b>	92.9	84.1	<b>97.1</b>	92.2	93.6	28.8	87.3
AdaptConnet	97.0	84.7	84.0	77.3	96.8	93.8	93.9	<b>84.8</b>	94.3	<b>93.1</b>	94.1	49.7	86.8
FMML w/o $\mathcal{L}_{mix}$	<b>97.8±0.03</b>	<b>88.5±0.03</b>	<b>90.5±0.02</b>	<b>86.4±0.02</b>	<b>90.3±0.02</b>	<b>92.2±0.03</b>	<b>92.8±0.02</b>	<b>84.3±0.03</b>	<b>97.1±0.02</b>	<b>92.4±0.01</b>	<b>91.1±0.02</b>	<b>47.6±0.02</b>	<b>87.5±0.03</b>
FMML w/o $\mathcal{L}_{ml}$	95.5±0.03	88.7±0.03	91.0±0.02	86.8±0.02	90.7±0.02	94.7±0.03	92.8±0.02	84.6±0.03	92.0±0.02	88.0±0.01	94.0±0.02	54.3±0.02	87.9±0.03
FMML	95.7±0.03	<b>88.8±0.03</b>	<b>91.3±0.02</b>	<b>86.9±0.02</b>	<b>90.9±0.02</b>	<b>94.8±0.03</b>	<b>92.9±0.02</b>	<b>84.8±0.03</b>	<b>92.0±0.02</b>	<b>88.5±0.01</b>	<b>94.2±0.02</b>	<b>55.7±0.02</b>	<b>88.1±0.03</b>

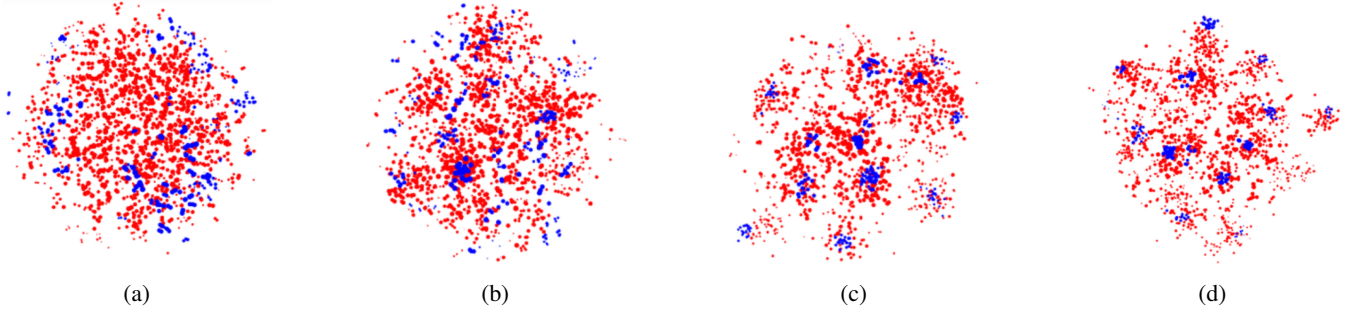


Figure 1: t-SNE visualization (best viewed in color) on task Amazon→DSL from Office-31 for a: pretrained ResNet-50, b: source-trained model, c: FMML on Source-Free, and d: FMML on Black-Box.

Table 5: Black-Box Domain Adaptation Accuracy(%) on Office-31 Dataset

Method	A→D	A→W	D→A	D→W	W→A	W→D	Avg.
Source-only	79.9	76.6	56.4	92.8	60.9	98.5	77.5
NLL-OT	88.8	85.5	64.6	95.1	66.7	98.7	83.2
NLL-KL	89.4	86.8	65.1	94.8	67.1	98.7	83.6
HD-SHOT	86.5	83.1	66.1	95.1	68.9	98.1	83.0
SD-SHOT	89.2	83.7	67.9	95.3	71.1	97.1	84.1
DINE	91.6	86.8	72.2	96.2	73.3	<b>98.6</b>	86.4
DINE-full	91.7	87.5	72.9	<b>96.3</b>	73.7	98.5	86.7
FMML w/o $L_{mix}$	92.0±0.20	87.8±0.10	72.9±0.07	95.1±0.10	73.9±0.07	98.0±0.20	86.8±0.05
FMML w/o $L_{ent}$	92.8±0.20	88.0±0.10	73.3±0.07	95.5±0.10	74.2±0.07	98.4±0.20	87.0±0.05
FMML	<b>93.0±0.20</b>	<b>88.2±0.10</b>	<b>73.5±0.07</b>	<b>95.8±0.10</b>	<b>74.4±0.07</b>	<b>98.5±0.20</b>	<b>87.2±0.05</b>

Table 6: Black-Box Domain Adaptation Accuracy(%) on Office-Home Dataset

Method	Ar→Cl	Ar→Pr	Ar→Rw	Cl→Ar	Cl→Pr	Cl→Rw	Pr→Ar	Pr→Cl	Pr→Rw	Rw→Ar	Rw→Cl	Rw→Pr	Avg.
Source-only	48.1	60.0	74.2	54.5	63.3	66.3	52.8	61.2	73.2	60.1	60.7	75.5	60.6
NLL-OT	49.1	71.7	77.3	60.2	68.7	73.1	57.0	46.5	76.8	67.1	52.3	78.5	64.9
NLL-KL	49.0	71.5	77.1	59.0	68.7	72.9	56.4	46.9	76.6	66.2	52.3	78.1	64.6
HD-SHOT	48.6	72.8	77.0	60.7	70.0	73.2	56.6	47.0	76.7	67.5	52.6	80.2	65.3
SD-SHOT	50.1	75.0	78.8	63.2	72.9	76.4	60.0	48.0	79.4	69.2	54.2	81.8	67.4
DINE	52.2	78.4	81.3	65.3	76.6	78.7	62.7	49.6	82.2	69.8	55.8	84.2	69.7
DINE-full	54.2	77.9	81.6	<b>65.8</b>	77.7	79.9	64.1	50.5	82.1	71.1	58.0	84.3	70.6
FMML w/o $L_{mix}$	54.0±0.02	78.0±0.02	81.9±0.02	64.8±0.04	78.2±0.02	79.7±0.02	64.3±0.04	50.7±0.02	82.3±0.02	71.8±0.04	58.1±0.02	84.4±0.02	70.8±0.02
FMML w/o $L_{ent}$	<b>55.0±0.02</b>	78.2±0.02	82.4±0.02	64.5±0.04	78.4±0.02	80.0±0.02	64.5±0.04	50.9±0.02	82.8±0.02	72.1±0.04	58.3±0.02	84.5±0.02	71.0±0.02
FMML	<b>55.0±0.02</b>	<b>78.5±0.02</b>	<b>82.8±0.02</b>	65.4±0.04	<b>78.7±0.02</b>	<b>80.1±0.02</b>	<b>64.7±0.04</b>	<b>51.2±0.02</b>	<b>83.0±0.02</b>	<b>72.4±0.04</b>	<b>58.6±0.02</b>	<b>84.6±0.02</b>	<b>71.3±0.02</b>

Table 7: Black-Box Domain Adaptation Accuracy(%) on VisDA-C Dataset

Method	plane	bicyc	bus	car	horse	knife	ncycl	person	plant	skated	train	truck	Mean
Source-only	64.3	24.6	47.9	75.3	69.6	38.5	79.0	31.6	64.4	31.0	81.4	92.7	48.9
NLL-OT	82.6	81.1	76.2	44.8	30.8	79.1	76.9	72.9	26.9	81.2	74.7	50.6	70.9
NLL-KL	82.7	83.4	76.7	44.9	30.9	38.5	78.4	71.6	82.4	80.3	82.9	50.4	71.9
HD-SHOT	75.8	85.8	78.0	43.1	32.0	41.0	79.9	78.1	84.2	86.4	81.0	65.8	74.2
SD-SHOT	79.1	85.8	77.2	45.4	31.6	41.0	80.0	78.3	84.7	86.8	81.1	65.1	74.5
DINE	81.4	86.7	77.9	<b>55.1</b>	32.2	24.6	<b>80.8</b>	<b>79.9</b>	87.3	87.9	84.3	58.7	75.6
DINE-full	<b>85.2</b>	85.9	80.1	53.4	33.0	37.7	80.7	79.2	86.3	<b>89.9</b>	85.7	60.4	77.3
FMML w/o $L_{mix}$	93.4±0.03	86.8±0.03	85.3±0.02	53.7±0.02	33.1±0.02	38.5±0.03	80.8±0.02	78.0±0.03	86.6±0.02	88.8±0.01	86.0±0.02	59.0±0.02	77.2±0.03
FMML w/o $L_{ent}$	94.4±0.03	86.5±0.03	79.8±0.02	54.6±0.02	33.3±0.02	40.4±0.05	79.2±0.02	78.1±0.03	87.2±0.02	89.5±0.04	86.6±0.02	59.8±0.02	77.6±0.03
FMML	94.0±0.03	<b>86.8±0.03</b>	79.8±0.02	55.0±0.02	<b>33.5±0.02</b>	<b>42.3±0.05</b>	80.2±0.02	78.6±0.01	<b>87.7±0.02</b>	89.5±0.02	<b>86.8±0.02</b>	59.5±0.02	<b>77.2±0.03</b>

Table 8: Comparison of Different Augmentation Methods for Black-Box Domain Adaptation

Method	A→D	Ar→Cl	Syn→Real
SD-SHOT	89.2	50.1	74.5
SD-SHOT w/ MixUp	89.5 (+0.3)	50.1 (+0.0)	73.6 (-0.9)
SD-SHOT w/ CutMix	89.0 (-0.2)	49.8 (-0.3)	74.2 (-0.3)
SD-SHOT w/ RandAugment	89.4 (+0.2)	50.3 (+0.2)	74.7 (+0.2)
SD-SHOT w/ <b>Frequency MixUp</b>	<b>90.8 (+1.6)</b>	<b>50.7 (+0.6)</b>	<b>75.2 (+0.7)</b>
DINE w/o MixUp	90.7	50.9	74.3
DINE (w/ MixUp by default)	91.6 (+0.9)	52.2 (+1.3)	75.6 (+1.3)
DINE w/ CutMix	91.0 (+0.3)	51.9 (+1.0)	74.4 (+0.1)
DINE w/ RandAugment	91.8 (+1.1)	52.0 (+1.1)	75.7 (+1.4)
DINE w/ <b>Frequency MixUp</b>	<b>92.3 (+1.6)</b>	<b>52.2 (+1.3)</b>	<b>76.0 (+1.7)</b>
DINE-full w/o MixUp	90.9	52.9	76.3
DINE-full (w/ MixUp by default)	91.7 (+0.8)	54.2 (+1.3)	77.3 (+1.0)
DINE-full w/ CutMix	91.4 (+0.5)	53.8 (+0.8)	77.1 (+0.8)
DINE-full w/ RandAugment	92.0 (+1.1)	54.4 (+1.5)	77.3 (+1.0)
DINE-full w/ <b>Frequency MixUp</b>	<b>92.8 (+1.9)</b>	<b>55.0 (+2.1)</b>	<b>77.6 (+1.3)</b>

ness of our method under these settings.

Table 9: Source-Free Partial-Set Domain Adaptation Accuracy(%) on Office-Home Dataset

Method	Ar→Cl	Ar→Pr	Ar→Rw	Cl→Ar	Cl→Pr	Cl→Rw	Pr→Ar	Pr→Cl	Pr→Rw	Rw→Ar	Rw→Cl	Rw→Pr	Avg.
Source-only	44.9	70.5	81.0	55.4	60.2	66.2	61.5	40.3	76.5	70.6	47.8	77.2	62.7
SHOTIM	59.1	83.9	88.5	72.7	73.5	78.4	75.9	59.9	90.3	81.3	68.6	88.7	76.7
SHOT	64.6	85.1	82.9	78.4	76.8	86.9	79.0	65.7	89.0	81.1	67.7	86.4	79.5
Source-only++	50.3	77.1	86.6	66.2	67.6	75.7	69.2	46.4	83.6	76.2	51.3	82.4	69.4
SHOTIM++	59.6	84.5	89.0	73.7	74.2	79.3	77.0	60.7	91.0	81.8	69.4	89.3	77.5
SHOT++	65.0	85.8	83.4	78.8	77.4	87.3	79.3	66.0	89.6	81.3	68.1	86.8	79.9
FMML	67.6	86.2	93.3	79.0	78.3	88.1	79.7	66.5	90.0	82.0	68.8	88.7	80.8

Table 10: Source-Free Open-Set Domain Adaptation Accuracy(%) on Office-Home Dataset

Method	Ar→Cl	Ar→Pr	Ar→Rw	Cl→Ar	Cl→Pr	Cl→Rw	Pr→Ar	Pr→Cl	Pr→Rw	Rw→Ar	Rw→Cl	Rw→Pr	Avg.
Source-only	36.3	54.8	69.1	33.8	44.4	49.2	36.8	29.2	36.8	31.4	35.1	62.3	46.6
SHOTIM	62.5	77.8	83.9	60.9	73.4	79.4	64.7	58.7	83.1	69.1	62.0	82.1	71.5
SHOT	64.5	80.4	84.7	63.1	75.4	81.2	65.3	59.3	83.3	69.6	64.6	82.3	72.8
Source-only++	36.7	55.9	69.9	34.2	44.7	49.0	37.7	29.5	36.6	30.2	33.7	62.5	46.7
SHOTIM++	62.3	78.4	82.9	60.3	73.1	78.9	64.1	58.2	82.8	68.7	62.2	82.3	71.2
SHOT++	65.8	79.4	83.5	62.9	73.6	80.4	65.4	59.7	83.3	69.3	64.8	82.0	72.5
FMML	67.0	80.8	85.4	64.0	73.8	80.6	65.9	60.0	84.6	69.5	65.6	82.5	73.4

Table 11: Black-Box Partial-Set Domain Adaptation Accuracy(%) on Office-Home Dataset

Method	Ar→Cl	Ar→Pr	Ar→Rw	Cl→Ar	Cl→Pr	Cl→Rw	Pr→Ar	Pr→Cl	Pr→Rw	Rw→Ar	Rw→Cl	Rw→Pr	Avg.
Source-only	44.9	70.5	81.0	55.4	60.2	66.2	61.5	40.3	76.5	70.6	47.8	77.2	62.7
DINE	58.1	83.4	89.2	78.0	80.0	80.6	74.2	56.6	85.9	80.6	62.9	84.8	76.2
DINE-full	55.6	79.0	85.3	75.3	77.6	78.5	74.1	56.7	83.8	78.4	59.6	83.1	73.9
FMML	60.0	84.2	89.7	78.0	80.8	80.6	74.9	57.4	86.8	80.5	63.3	85.1	76.8

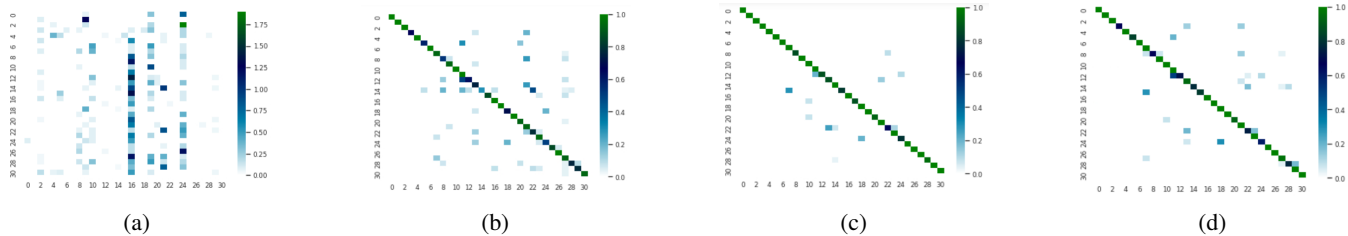


Figure 2: Confusion matrix (best viewed in color) on task Amazon→DSLRL from Office-31 for **a**: pretrained ResNet-50, **b**: source-trained model, **c**: FMML on Source-Free and **d**: FMML on Black-Box.

Table 12: Black-Box Open-Set Domain Adaptation Accuracy(%) on Office-Home Dataset

Method	Ar→Cl	Ar→Pr	Ar→Rw	Cl→Ar	Cl→Pr	Cl→Rw	Pr→Ar	Pr→Cl	Pr→Rw	Rw→Ar	Rw→Cl	Rw→Pr	Avg.
Source-only	36.3	54.8	69.1	33.8	44.4	49.2	36.8	29.2	36.8	31.4	35.1	62.3	46.6
DINE	52.4	80.7	86.4	75.6	77.7	78.5	72.6	52.9	83.9	78.4	60.4	82.8	73.2
DINE-full	51.0	78.5	84.7	74.7	75.9	77.0	71.0	50.4	82.9	77.6	60.2	81.1	72.1
FMML	53.7	82.0	87.3	75.5	77.1	79.0	73.4	53.6	84.4	78.8	60.6	83.1	74.1

## 5. Full Comparisons between Vanilla MixUp and Frequency MixUp

In this section, vanilla MixUp (?) is compared with Frequency MixUp and results are shown in Table 13-18. Here strong baselines SHOT++ (?) and DINE-full (?) are applied. Frequency MixUp provides a gain of 1.5% and 2.6% for Source-Free and Black-Box on Office-31, while vanilla MixUp causes an increase of 0.3% and 1.1% on it. Frequency MixUp provides a gain of 0.7% and 1.1% for Source-Free and Black-Box on Office-Home, while vanilla MixUp causes an increase of 0.1% and 0.7% on it. Frequency MixUp provides a gain of 0.6% and 1.3% for Source-Free and Black-Box on VisDA-C, while vanilla MixUp causes an increase of -0.5% and 1.0% on it. Our experiments show that Frequency MixUp outperforms vanilla MixUp.

Table 13: MixUp Comparisons for Source-Free on Office-31 Dataset

Method	A→D	A→W	D→A	D→W	W→A	W→D	Avg.
SHOT++	94.3	90.4	76.2	98.7	75.8	99.9	89.2
SHOT++ w/ MixUp	94.5	91.4	76.3	99.0	76.1	99.9	89.5
SHOT++ w/ Frequency MixUp	95.2	95.0	77.4	99.0	77.3	100	90.7

Table 14: MixUp Comparisons for Source-Free on Office-Home Dataset

Method	Ar→Cl	Ar→Pr	Ar→Rw	Cl→Ar	Cl→Pr	Cl→Rw	Pr→Ar	Pr→Cl	Pr→Rw	Rw→Ar	Rw→Cl	Rw→Pr	Avg.
SHOT++	37.9	79.7	82.5	68.5	79.6	79.3	68.5	57.0	83.0	73.7	60.7	84.9	73.0
SHOT++ w/ MixUp	38.4	80.0	82.5	68.7	79.8	79.8	68.8	56.9	82.9	73.4	60.5	85.1	73.1
SHOT++ w/ Frequency MixUp	39.4	81.1	83.5	69.3	80.2	80.5	69.2	58.4	82.9	73.1	61.1	85.5	73.7

Table 15: MixUp Comparisons for Source-Free on VisDA-C Dataset

Method	plane	bicycl	bus	car	horse	knife	mcycl	person	plant	sktbrd	train	truck	Mean
SHOT++	97.7	88.4	90.2	86.3	97.9	98.6	92.9	84.1	97.1	92.2	93.6	28.8	87.3
SHOT++ w/ MixUp	94.8	88.0	89.7	86.4	90.5	95.0	92.9	83.2	93.5	87.6	93.9	35.1	86.8
SHOT++ w/ Frequency MixUp	95.5	88.7	91.0	86.8	90.7	94.7	92.8	84.6	92.0	88.8	94.0	54.3	87.5

Table 16: MixUp Comparisons for Black-Box on Office-31 Dataset

Method	A→D	A→W	D→A	D→W	W→A	W→D	Avg.
DINE-full w/o MixUp	90.7	86.0	70.2	95.2	73.0	98.2	85.6
DINE-full (w/ MixUp by default)	91.7	87.5	72.9	96.3	73.7	98.5	86.7
DINE-full w/ Frequency MixUp	92.8	88.0	73.3	95.5	74.2	98.4	87.0

Table 17: MixUp Comparisons for Black-Box on Office-Home Dataset

Method	Ar→Cl	Ar→Pr	Ar→Rw	Cl→Ar	Cl→Pr	Cl→Rw	Pr→Ar	Pr→Cl	Pr→Rw	Rw→Ar	Rw→Cl	Rw→Pr	Avg.
DINE-full w/o MixUp	30.9	76.8	81.0	63.2	77.2	79.4	64.0	49.7	82.1	72.8	58.1	84.5	69.9
DINE-full (w/ MixUp by default)	54.2	77.9	81.6	65.9	77.7	79.9	64.1	50.5	82.1	71.1	58.0	84.3	70.6
DINE-full w/ Frequency MixUp	55.0	78.2	82.4	64.5	78.4	80.0	64.5	50.9	82.6	72.1	58.3	84.5	71.0

Table 18: MixUp Comparisons for Black-Box on VisDA-C Dataset

Method	plane	bicycl	bus	car	horse	knife	mcycl	person	plant	sktbrd	train	truck	Mean
DINE-full w/o MixUp	92.6	84.7	77.8	78.0	53.5	91.5	35.6	77.8	86.0	89.8	85.4	34.2	76.3
DINE-full (w/ MixUp by default)	95.3	85.9	80.1	53.4	93.0	37.7	80.7	79.2	86.3	89.9	85.7	60.4	77.3
DINE-full w/ Frequency MixUp	94.4	86.5	79.0	54.6	93.3	40.4	79.2	78.1	87.2	89.5	86.6	55.8	77.6

## 6. Confusion Matrix Visualization

Confusion matrices of three situations (i.e. pretrained ResNet-50, source-trained model, and our model FMML) with the task Amazon→DSLRL from the Office-31 (?) dataset are shown in Fig. 2. Subfigure a is the result of pretrained ResNet-50, which shows a random distributions. Subfigure b shows the result of source-trained model. Subfigure c and d represents the result of our model FMML on Source-Free and Black-Box settings. From these confusion matrices, we observe that training on source can obtain meaningful models, and further adaptations via our approach help improve the performance.